Applications and techniques of high, ultra high and extreme vacuum technology

An introduction to vacuum technology

Sally Marcher

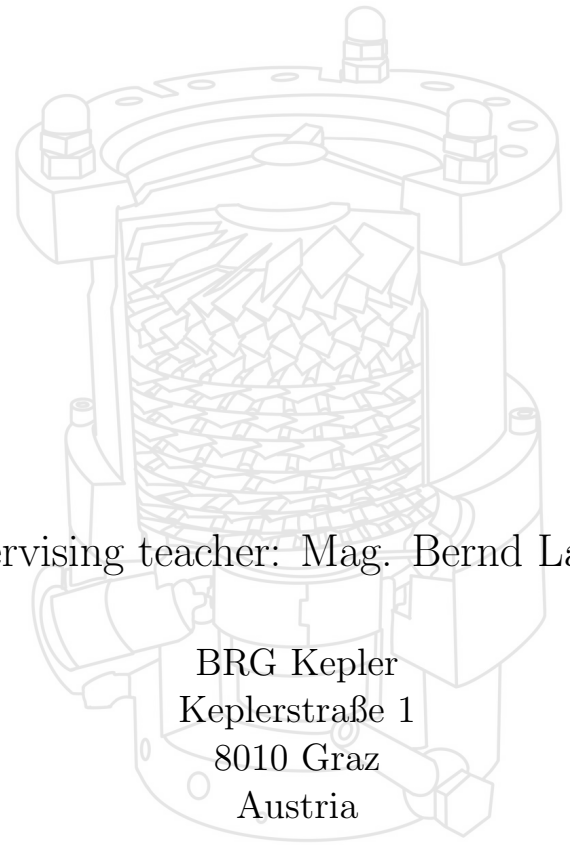

Supervising teacher: Mag. Bernd Lackner

BRG Kepler
Keplerstraße 1
8010 Graz
Austria

1st March 2024

Abstract

Understanding the behavior of pressure within high vacuum systems is paramount for the design and operation of vacuum equipment across diverse applications. This paper presents an experimental investigation aimed at elucidating the dynamics of pressure reduction in a comprehensive vacuum setup comprising roughing pumps, high vacuum pumps, and measurement devices. Emphasizing the theoretical underpinnings, particularly regarding vacuum gauges, this study underscores the significance of comprehending principles before embarking on experimental endeavors.

The practical part of this paper describes the construction of a high-vacuum setup and possibilities to simulate this process. However, limitations were evident, particularly under higher pressures and during the startup phase of the turbomolecular pump. Practical considerations, such as seal performance, were thoroughly addressed, suggesting avenues for enhancement in future setups.

Moreover, this research underscores the enduring relevance of vacuum technology in contemporary contexts, emphasizing its indispensable role across various fields up until the present day.

Contents

1. Introduction

Vacuum Technology is a complex and multifaceted science that requires a basic understanding of classical physics to comprehend its underlying principles. This paper aims to dissect this intricate subject into smaller, more digestible chapters.

The first chapter will delve into vacuum pumping technology, distinguishing between roughing pumps and (ultra) high vacuum pumps. Understanding the different air flow modes and their corresponding particle interactions is essential for grasping the concepts explored in subsequent chapters.

Particle interactions vary across different pressure ranges, necessitating the use of specific vacuum measurement devices tailored to each range. This paper will explore capacitive, Pirani, and crossed field gauges, which form a robust combination of gauges commonly used together, as evidenced by their availability in combined units today [25].

Additionally, practical applications of vacuum technology will be examined, particularly its pivotal role in chip manufacturing and various essential industries.

Finally, the construction of a basic high vacuum setup on a limited budget will be addressed. Practical experience is indispensable for understanding such advanced technological concepts. The deliberate focus on budget constraints is chosen to provide a unique perspective, as constructing a vacuum setup with standard parts alone would yield a less nuanced understanding.

2. Insight into different types of vacuum, high vacuum and ultra high vacuum pumps

2.1. Roughing pumps

2.1.1. Rotory vane pumps

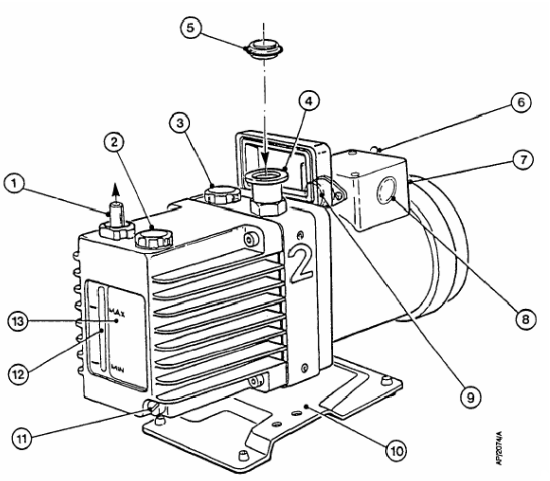

Figure 2.1.: Edwards E2M2 rotory vane pump [4].

Rotory vane pumps or sliding vane pumps, such as the one depicted in figure 2.1 are oil sealed pumps designed for both long term industrial applications and laboratory use. Oil is used for sealing the rotory vanes to the housing of the rotor [4].

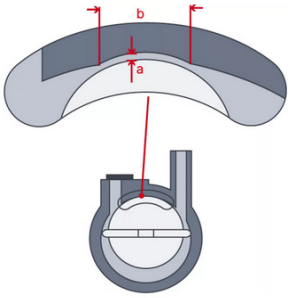

Figure 2.2.: Simplified schematic of a 1-staged rotory vane pump [30].

Figure 2.2 shows the rotor (white) and stator (dark grey). If the rotor spins, the gas volume (light grey) first increases while the inlet port (on the right side) is open and then decreases with the outlet port accessable to the gas volume. Thereby pumping is achieved [30].

The distance a should be as small as possible, while the distance b should be as large as possible to achieve a good seal between inlet and outlet. Oil is mandatory in such a system in order to decrease wear on the rotory vanes, while power is needed to spin the reotor and improve the seal [30].

Multiple stages can be connected inside in one pump to achieve higher vacuum levels. For use as a roughing pump for small turbo molecular pumps, only 2- or 3-staged pumps are used, as cheap 1-staged pumps often cannot achieve the desired level of vacuum, falling into the fine to high vacuum range [30].

One of the big disatvantages of such pumps is the need for oil lubrication. Oil could get into the ultra high vacuum system part of such a system and contaminate expensive parts with oil. Cleaning such parts is often a lengthy and expensive procedure [30].

2.1.2. Scroll Pump

In contrast to the widly used rotory vane pump, this vacuum pump is "dry" (without oil lubrication) and therefore there is no risk of contamination [20].

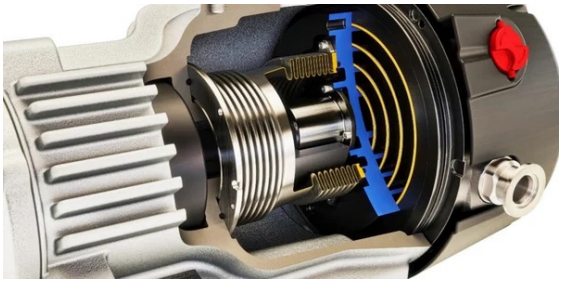

Figure 2.3.: Scroll pump inner workings [20].

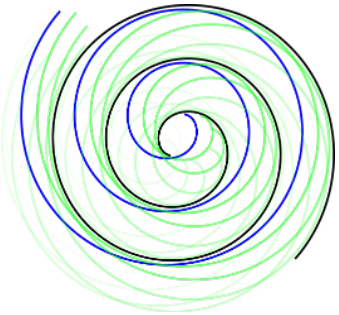

Figure 2.4.: Scroll pump pumping unit crossection. Source: Sally Marcher

Both the stator (black) and rotor (blue) in Figure 2.4 are spirals. The rotor spins with the motion illustrated by the green spirals. Compared to other vacuum pumps these types are also lower noise, lower vibration and lower operational costs, but the initial buying cost is higher. These pumps are also more sensetive to debris entering the inlet port [20].

Research shows that such pumping devices additionally come with a lower final pressure and buying used pumps on the second hand market is also more expensive compared to sliding vane pumps.

2.1.3. Diaphragm Pumps

Another completely oil free vacuum pump is the diaphragm (or membrane) pump. Even if the pumping speed is lower than scroll pumps, the field of application is similar. Both pumps offer great resilience against solvents. The diaphragm pump can be considered a smaller alternative to a scroll pump [22].

Figure 2.5.: Membrane pump [22].

The operational principle is comparable to conventional cylinder based pumps, but

instead of a sliding motion, a diagphragm is used to improve the seal. The higher ultimate pressure of 0.5mbar (2-staged pumps) makes it possible to use for newer turbo molecular pumps with a different pumping mechanism, as a backing pump which will further be illustrated in section 2.2.2.

Older TMPs usually need 10^{-2}mbar or lower, therefore for most used turbo pumps, affordable for makers, these pumps are no option for backing purposes [31].

2.1.4. Other types

There are numerous other types of vacuum pumps, such as screw pumps and roots vacuum pumps. However these are not explained in this paper, as I had minimal to no contact with such pumps during the construction of my low-cost ultra high vacuum setup, as they are either too expensive on second hand markets, just too new to get phased out by industry or educational institutions or way too big and heavy for my application.

2.2. (Ultra) High vacuum pumps

This subsection will discuss vacuum pumps capable of achieving high and ultra-high vacuum levels. The distinction between these is not entirely clear, as all the pumps under consideration can attain ultra-high levels of vacuum. The key factors influencing this achievement are the materials used, the quality of seals, cleanliness, and the potential use of oil in the pumps.

At such low pressures, the process of pumping shifts from simply moving gas from one place to another to the more challenging task of capturing gas molecules. You can picture roughing pumps as repeatedly reaching into a swimming pool filled with rubber balls. When dealing with a large number of constantly moving rubber balls, this method works effectively. However, as the number of rubber balls decreases, the probability of success diminishes significantly, to the point where it becomes extremely unlikely, if not almost impossible. This is precisely why high-vacuum pumps prioritize the capture and removal of particles. It also explains why high-vacuum flanges, like CF flanges, are notably larger in comparison to their low-vacuum counterparts.

2.2.1. Oil diffusion pump

Oil diffusion pumps are among the most cost-effective options, primarily due to their age rather than their economic efficiency. Their functioning is based on vaporizing synthetic oil, allowing it to rise as oil vapor, directing the flow through the use of the so called pump stack, and then condensing back into liquid to capture air molecules. In the liquid form the molecules then return to the heater, where the boiling process begins anew. In this delicate interplay, the condensation phase captures various gases, while the liquid's transformation during vaporization releases the trapped gases again. Since they do not have any moving parts or high voltage, these pumps are much safer to operate than turbo molecular or ion getter pumps. Diffusion pumps are also resistant to mechanical stress and vibrations. The only downside is the somewhat expensive oil that needs to be changed regularly, especially for applications with high gas flow [21].

Further advantages, are the consistent pumping speed below 10^{-3} mbar and minimal dependence on the gas type for pumping speed. However, a notable drawback emerges from the presence of oil that can infiltrate the high vacuum chamber. This concern can be alleviated by employing water cooled oil baffles [9].

Figure 2.6.: Oil diffusion pump. Source: Sally Marcher

Figure 2.7.: Diffusion Pump stack. Source: Sally Marcher

Figure 2.8.: Diffusion Pump Baffle. Source: Sally Marcher

2.2.2. Turbomolecular pump

The turbomolecular pump (often refferd to as a TMP) features a single rotor rotating at speeds ranging from 36,000 to 72,000 rpm and comprises multiple stages designed to transfer rotational energy to gas molecules in the form of an impulse, directing them toward the pumping direction. Rotational speeds of that kind have to be achieved, cause the transferred speed has to be greater than the average thermal velocity of the pumped particles which can be discribed by the formula $\bar{c} = \sqrt{\frac{8 \cdot R \cdot T}{\pi \cdot M}}$ [12].

With such high rotational speeds, it becomes increasingly challenging to develop bearings that can withstand these velocities. Over the nearly 100-year-long history of development, several successful bearing concepts have emerged. Among the well-known ones are oil-lubricated steel ball bearings, grease-lubricated hybrid bearings, and magnetic levitation bearings, which eliminate the need for lubrication entirely. The issue with steel bearings was that, in the absence of a lubrication oil film, microwelding could occur at points of contact. To mitigate this problem, hybrid bearings incorporate a steel shell with ceramic bearings. One of the most elegant solutions involves magnetically levitating bearings. These bearings require absolutely no lubrication. In older models, large electromagnets and complex circuitry were used to balance the rotor. However, with the use of permanent magnets and more advanced electronics, this technique has now become widespread and compact [12].

Figure 2.9.: Me swapping out a TMP. Source: Sally Marcher

Figure 2.10.: Disassembled TMP. Source: Sally Marcher

Figure 2.11.: Broken (left part) TMP rotor. Source: Sally Marcher

In Figure 2.9, I replaced an old Alcatel 5150 with a newer and faster Leybold TURBOVAC 360c. Both feature 25 ISO-KF flanges, eliminating the need for adapters. The construction of Turbo Pumps is depicted in Figures 2.10 and 2.11. The rotor spins at peripheral speeds of up to 400 meters per second, while the stator blades remain station-

ary. Any particles that enter the turbo molecular pump will be caught by the spinning rotor. The impact will cause an elastic colission between the solid rotor and the gas [27].

$$v_{roti} \approx v_{rotf} \tag{2.1}$$

$$v_{pf} \approx v_{roti} \times 2 \tag{2.2}$$

where:

v_{roti} ... Initial rotor speed
v_{rotf} ... Final rotor speed
v_{pf} ... Final particle speed

The gas particle, as described by simplifying the elastic collision theory in equations (2.1) and (2.2), therefore gains twice the speed of the rotor. These simplifications are permissible because the rotor has a significantly greater mass compared to the target gas molecule [16].

Viewed within a three-dimensional system, a problem arises: particles would not gain speed in the required direction. To address this, stator blades were introduced, redirecting the impulse and gradually decelerating the particle at each stage. Each stage implements a different angle of attack. The variation in that regard is determined by the pressure exerted on the blade, with a reduced angle of attack resulting in less force on the blade but also less pumping speed. The final configuration of the blade layout varies among manufacturers, and developing efficient blade layouts often necessitates simulations that would exceed the scope of this paper.

Various pumping mechanisms have been developed. Figure 2.11 displays a "classic rotor" that was damaged due to a break in the line connected to the fore pump.

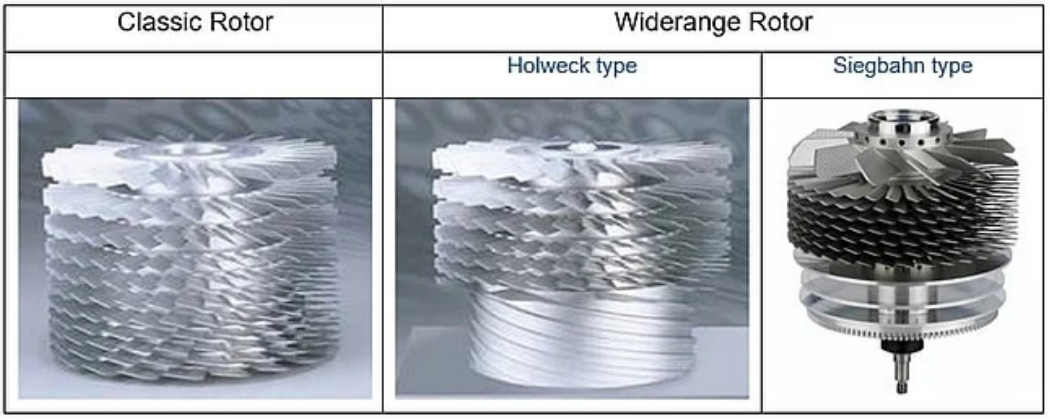

Figure 2.12.: Different pumping mechanisms [19].

As certain roughing pumps fail to achieve the necessary operating pressures for turbo molecular pumps due to increased rotor speeds and reduced operating pressures re-

quired, alternative pumping mechanisms were developed. The "Classic Rotor" became insufficient for these demands. The developed mechanisms are depicted in Figure 2.12. The "Widerange Rotor" enabled the utilization of smaller oil-free pumps, such as the diaphragm pump (Figure 2.5), as backing pumps [19].

3. Insight into different types of vacuum measurment devices

Measuring vacuum is considered one of the more challenging tasks in high vacuum physics since mainstream pressure measurement devices do not effectively operate at such low pressures.

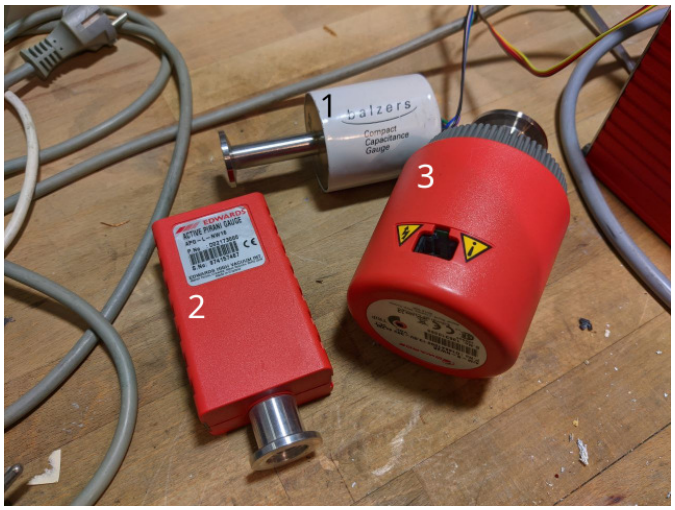

Figure 3.1.: Different vacuum sensors. Source: Sally Marcher

Figure 3.1 depicts three different vacuum sensors. With these three sensors, pressures ranging from $1 \cdot 10^{-9}$ mbar [7] up to 1100 mbar [17] can be measured with acceptable accuracy:

1. Capacitive pressure sensor
2. Pirani pressure sensors
3. Inverted magnetron gauge

3.1. Capacitive pressure sensors

The Sensor 1 in Figure 3.1 operates by deflecting a ceramic diaphragm due to pressure, which is then measured capacitively. Enhanced accuracy is attained by heating the diaphragm to maintain a constant temperature [17].

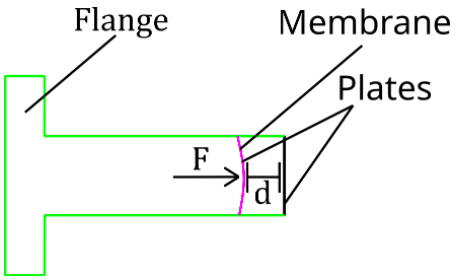

Figure 3.2.: Capacitive pressure sensor. Source: Sally Marcher

Pressure can be described as [16]

$$p = \frac{F}{A} \tag{3.1}$$

where:

p ... Pressure
F ... Force
A ... Area

In capacitance sensors, the area of the membrane remains relatively insignificant across the pressure range. However, due to the force acting on the membrane, the distance between the plates alters. Consequently, the average distance between the membrane and a flat surface is capacitively measured, this effect can also be seen in plate capacitors desribed in equation (3.2) [16].

$$C = \frac{\varepsilon \cdot A}{d} \tag{3.2}$$

where:

C ... Pressure
ε ... Permittivity constant
A ... Area of the plate
d ... Seperation distance

The more challenging task regarding such sensors is measuring the capacity; for that, these sensors utilize the change in impedance at a certain frequency. This is described by equation (3.3) [10].

$$Z_C = \frac{1}{\omega \cdot C} \tag{3.3}$$

where:

Z_C ... Impedance of capacitor at angular frequency ω
ω ... Angular frequency
C ... Capacity

$$V = V_{in} \frac{R_2}{R_1 + R_2} \tag{3.4}$$

where:

V ... Output Voltage
V_{in} ... Input Voltage
R_1 ... Resistor 1
R_2 ... Resistor 2

For measuring the impedance, we can construct a voltage divider [10] as described in equation (3.4). This involves replacing the second resistor with the capacitor, as illustrated in figure 3.3.

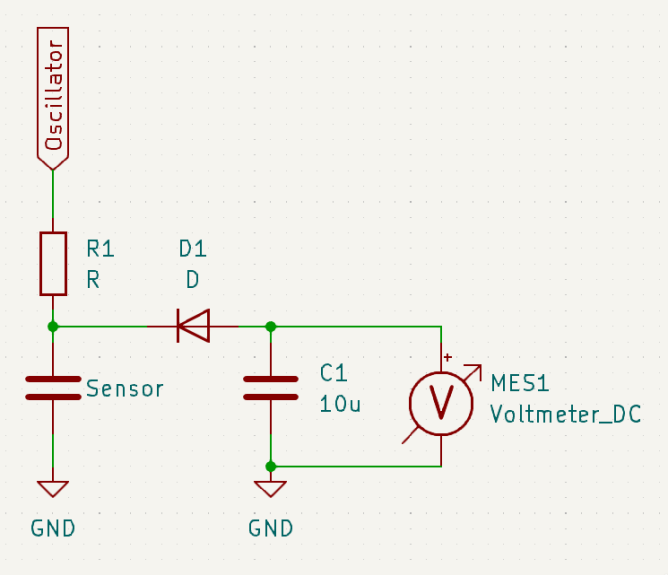

Figure 3.3.: Capacitive measurment circuit. Source: Sally Marcher

If we substitute equation (3.3) for R_2 in equation (3.4), we can derive a formula describing the capacitance C.

$$C = \frac{V_{osc} - V_{meter}}{V_{meter} \cdot R_1 \cdot 2\pi f} \tag{3.5}$$

where:

C ... Capacity of the sensor
V_{osc} ... Peak voltage of the oscillator
V_{meter} ... Measured voltage
R_1 ... Resistor 1
f ... Frequency of the oscillator

The capacitance can therefore be measured simply by monitoring the voltage, allowing for the achievement of pressure measurements.

3.2. Pirani pressure sensors

Pirani sensors are especially well-suited to measure small changes in pressure. The gauge works via the change in heat conductivity when pressure changes by using different heat conduction modes [1].

The heating of the gas works electrically by passing a current through a small wire, the emitted power can therefor be described in equation (3.6).

$$\dot{Q}_{el} = UI \tag{3.6}$$

where:

$\dot{Q}_{el}$ ... Electrical Power
U ... Voltage
I ... Current

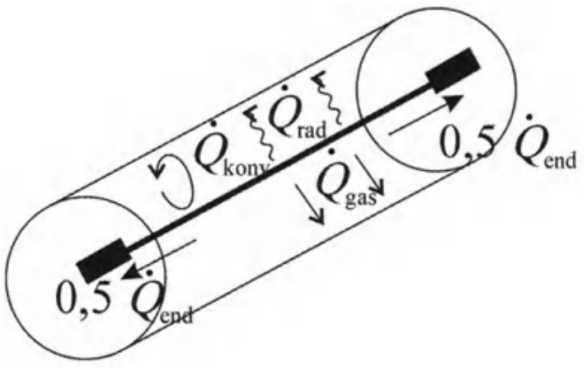

Figure 3.4.: Heat flux system in a pirani gauge [11].

All the energy must leave the system for the wire to maintain a constant temperature. This occurs in four different modes [11]:

$$\dot{Q}_{el} = \dot{Q}_{gas} + \dot{Q}_{end} + \dot{Q}_{rad} + \dot{Q}_{conv} \tag{3.7}$$

1. Heat flux $\dot{Q}_{gas}$ occurs through the gas between the heated wire ($T_1 \approx 400K$) and the wall at room temperature ($T_2 \approx 300K$). The energy flow or the dissipated heat power in the molecular flow region is proportional to the pressure p. In the viscous flow region, $\dot{Q}_{gas}$ is independent of pressure. In the transition region, the pressure dependence of $\dot{Q}_{gas}$ can be well described by equation (3.8).

2. Heat flux $\dot{Q}_{end}$ occurs through the fixtures of the wire.

3. Heat flux through radiation $\dot{Q}_{rad}$.

4. Heat flux $\dot{Q}_{conv}$ caused by convection at pressures $> 10mBar$.

$$\dot{Q}_{gas} = \varepsilon \frac{p}{1 + g \cdot p} \tag{3.8}$$

where:

$\dot{Q}_{gas}$ ... Heat flux caused by gas
ε ... Sensitivity (Depends on the gas type)
g ... Geometry
p ... Pressure

The convective heat flux ($\dot{Q}_{conv}$) is contingent upon numerous factors, including emission rate, geometry, and the temperature distribution along the wire. Consequently, its calculation is inherently challenging. Under conditions of extremely low pressures, where the contribution of convective flux ($\dot{Q}_{conv}$) becomes negligible, the behavior of heat flux ($\dot{Q}_{gas}$) can be elucidated through equation (3.9) [11].

At pressures exceeding this threshold, measurements are typically conducted using calibration curves.

$$\dot{Q}_{el} = \varepsilon \cdot (p_0 + \frac{p}{1 + g \cdot p}) \tag{3.9}$$

where:

$\dot{Q}_{el}$ ... Total heat flux (electrical power)
ε ... Sensitivity (Depends on the gas type)
p_0 ... zero point calibration value
g ... Geometry
p ... Pressure

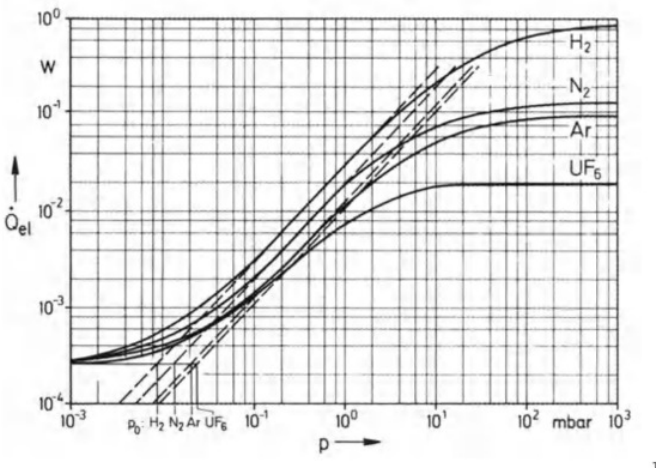

Figure 3.5.: Electrical power ($\dot{Q}_{el}$) needed for constant temperature [11].

The emission power (equation (3.6)) is determined through the measurement of the wire's resistance, which is directly proportional to the temperature of the wire. This temperature, in turn, is proportional to the total heat flux. This is usually done using a Wheatstone bridge and operational amplifiers [11].

3.3. Crossed field gauges

The last of the three sensors is of the "inverted magnetron" type. These sensors are part of a broader category known as crossed-field gauges. Almost all available commercial crossed field gauges are of the Penning design or of the Redhead and Hobson design as magnetron or inverted magnetron [6].

To gain a comprehensive understanding of inverted magnetron gauges, it is essential to first examine an earlier type of crossed-field gauge—the Penning gauge.

3.3.1. The Penning gauge

This gauge operates by applying a high DC voltage (approximately 3000V) between a cathode and an anode. The resulting current from this discharge is dependent on the pressure. However, this method is effective only down to approximately 1 Pa, as at this level, the gas density becomes too low to sustain the discharge. This gauge type got its name from the magnetic field, that crosses the electric field. That forces the electrons to take a spiral path, thus making it possible to maintain a discharge down to a lower pressure [11].

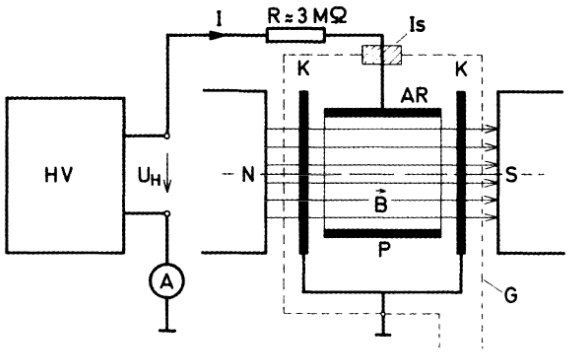

Figure 3.6.: Penning gauge schematic [11].

Figure 3.6 illustrates the fundamental structure of a Penning gauge. The high voltage ($U_H \approx 3kV$) is generated by the HV supply. The resistor serves to limit the current flow, particularly at elevated pressures.

The anode (AR) is configured in the shape of a pipe, with plates acting as cathodes located at each end. The magnetic field, denoted as $\vec{B}$, is arranged to ensure nearly homogenous field lines through and parallel to the pipe. The discharge current I is measured using an ampere meter (A).

In any case, the magnetic field (B = 0.1 T to 0.2 T) is crucial for the discharge mechanism, as it significantly hinders the movement of electrons perpendicular to the field lines, towards the anode (figure 3.6), therefore a electron space charge is formed.

Through collisions with air molecules, electrons can gradually advance toward the anode. This diffusion effect towards the anode is significantly impeded by the magnetic field. Simultaneously with the diffusion process, another phenomena that occurs is ionization colission. In this scenario, a gas molecule becomes ionized, releasing an electron that becomes incorporated into the electron space charge. However, the ion itself cannot be integrated as its orbital radius is larger than that of the electron, resulting in it promptly reaching the anode.

In figure 3.7, a typical calibration curve is presented, also illustrating why crossed-field gauges typically operate only up to a pressure of 10^{-2} mBar. At this point, the gas density reaches a level where the plasma begins to dominate over the electron ring [11].

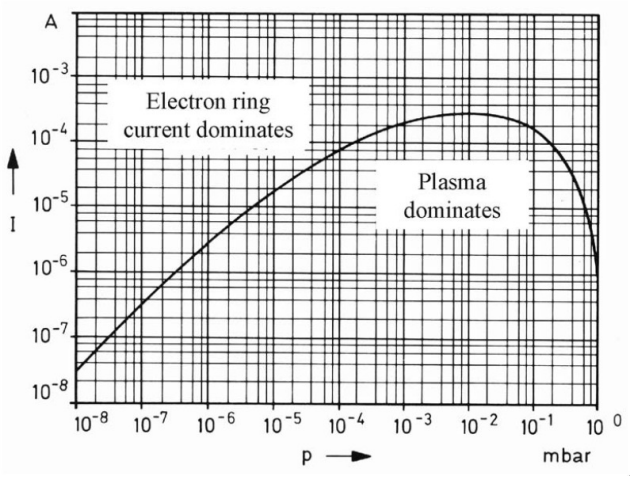

Figure 3.7.: Typical Penning gauge calibration curve [6].

3.3.2. The inverted magnetron gauge

The inverted magnetron gauge improves upon the classical penning gauge design, making the trapping of electrons more effective, thus sensitivity is improved and the operational region is extended to a lower pressure of 10^{-11} mBar. The main improvments are a new anode design and a guard ring (auxiliary cathode in figure 3.8) to prevent unwanted field emissions [6].

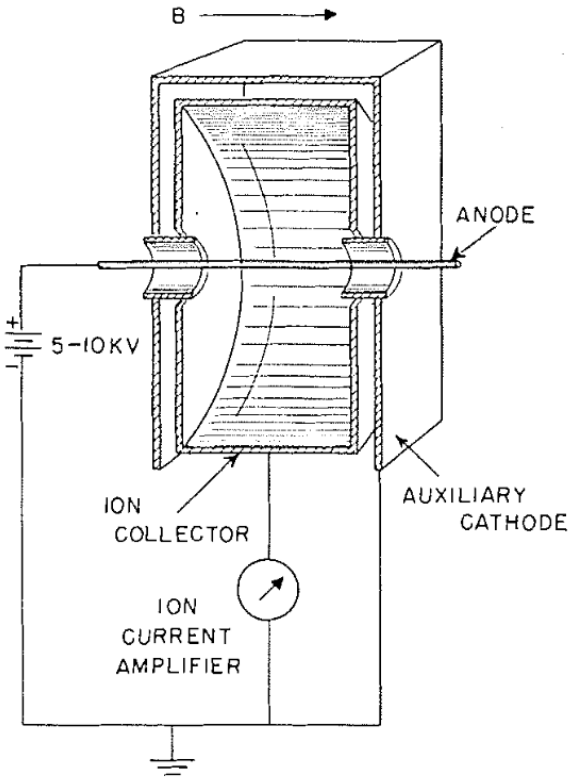

Figure 3.8.: Inverted magnetron schematic [2].

The preceding section is equally applicable to this type of gauge. However, it is crucial to note that those theories have tended to overlook the dynamics of electron space charges. These charges manifest as large amplitude RF oscillations, capable of modifying the static system. The introduction of this AC field allows excess-energy electrons to readily impact the cathodes (in Penning gauges) or the cathode end plates (in inverted magnetron gauges). These interactions introduce non-linearities in the current-pressure curve and may lead to significant disturbances in the output if unintentionally amplified in the ion-current amplifier. This is where the inverted magnetron comes into play, as its modified magnetic field design reduces these effects and contributes to an overall reduction in size compared to the magnetron gauge [6].

4. Practical Applications

The techniques for producing and measuring high vacuum have been elucidated in the preceding two chapters, but now the practical applications must be discussed. Vacuum technology has witnessed an expansion of applications over the last 20 years. However, paradoxically, the number of scientists working in vacuum technology has been deveasing annually. The development in this field has primarily been evolutionary rather than revolutionary, with a predominant focus on engineering efforts over scientific endeavors [11].

Due to the intricate nature and extensive scope of the given examples, comprehensive explanations of them are deemed impractical within the confines of this paper, given their specialized domains.

4.1. Chip manufacturing

4.1.1. EUV Lithography

Extreme Ultraviolet (EUV) lithography has emerged as an industrial standard for chip manufacturing. Since 2018, high-volume manufacturing has become feasible with the EUV scanners developed by ASML. Leading industrial manufacturers such as Samsung, TSMC, and Intel have already integrated EUV technology into their modern processes. The necessity for this technology arises from its small wavelength of only 13.5 nm, crucial for producing technology nodes beyond 7 nm [18].

Figure 4.1.: Internal structure of ASML NXE:3400B scanner [18].

As illustrated in figure 4.1, both the reflection system and the EUV light source operate under a high-vacuum atmosphere. This condition is essential to prevent high absorption on the EUV optical path and to maximize the reflectivity of the first-surface mirrors [18].

High-NA EUV Litography

As of February 2024, ASML has delivered the new high-NA EUV lithography machine to Intel [24].

Figure 4.2.: Mirror testing facility from ZEISS with vacuum chambers measuring a diameter of five meters [29].

The enhanced high-NA EUV lithography system is even more sensitive to turbulence-induced measurement noise. Zeiss, in response, has constructed new colossal vacuum chambers for mirror production, utilizing vapor deposition. To grasp the precision required, envision scaling up the mirror size to that of Germany, where the largest unevenness must be less than 100 micrometers. Such exacting specifications necessitate the entire process to be conducted under vacuum conditions, as the presence of air would render vapor deposition and measurements at this level of precision impossible [29].

4.2. Analytics

The low pressure in high vacuum produces an extremely long mean free path. Therefore it presents some specific possibilities for analytics in the fields of surface science, thin film deposition, and particle physics. Enabling precise control and characterization of molecular interactions, atomic layer deposition processes, and the study of rarefied gas dynamics, respectively.

4.2.1. Scanning Electron Microsopes

Optical Microscopes (OM) encounter resolution limits regarding their precision. While it may seem that infinitely precise lenses could yield infinite resolution, several less obvious

factors come into play, most notably the wavelength of light and the characteristics of the light source. These factors have prompted scientists to develop a new kind of microscope that operates at significantly higher magnification and experiences less diffraction. Consequently, for the first time, particles in the nanometer size range could be resolved [15].

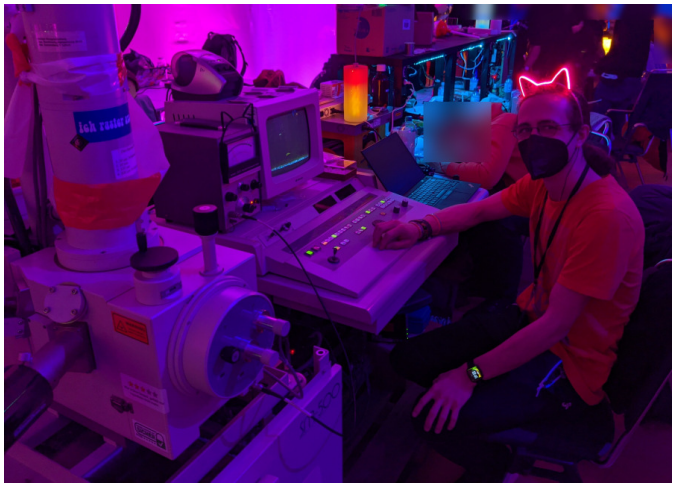

Figure 4.3.: An operational SEM at CCC Congress 2023. Source: Sally Marcher

Scanning electron microscopes (as depicted in figure 4.3), as well as transmission electron microscopes, must operate under high vacuum conditions. Interactions between gas molecules and electrons would render such high resolution impossible. The components maintained under vacuum include the test chamber, illustrated in figure 4.4, and the column for magnetic field lenses [15].

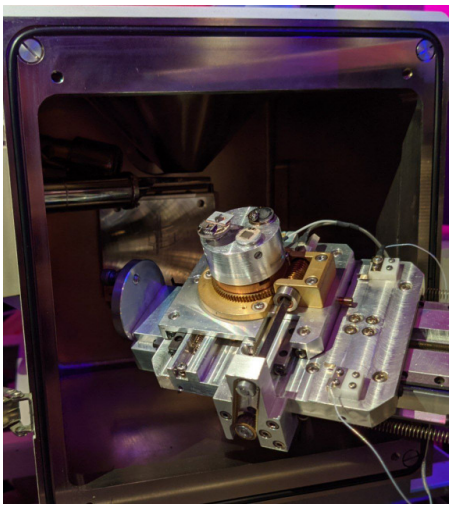

Figure 4.4.: Probe chamber of the microscope. Source: Sally Marcher

4.2.2. Mass spectrometers

Figure 4.5.: The treasure islands of MS [13].

"A modern mass spectrometer is constructed from elements which approach the state-of-the-art in solid-state electronics, vacuum systems, magnet design, precision machining, and computerized data acquisition and processing" [3] This exact quote, from a 1979 paper by W. V. Ligon, remains true to this day, illustrating the rapid and continuous development of new techniques, machines, and processes [13].

Mass spectrometers separate ions by mass. This separation can occur in various ways, as depicted in figure 4.5. In the graphic representation, the boundaries between these types are not clearly defined. Many modern mass spectrometers integrate multiple principles, as illustrated by the pathways between the islands in the figure. However, the vacuum system is an integral part of all mass spectrometers. Without vacuum, it would not be possible to operate any mass spectrometer because the required mean free path for the ions would not be achievable.

Figure 4.6.: Balzers quadrupole gas analyzer. Source: Sally Marcher

Figure 4.6 depicts a gas analyzer manufactured by Balzers. The measurement head must be under vacuum, thus the analyzer can be connected via the flange to a system.

4.3. Thin film technology

Thin film technology is primarily utilized to enhance material properties. Examples of these properties include transmission, reflection, absorption, hardness, abrasion resistance, corrosion resistance, permeation, and electrical characteristics. Additionally, nanotechnology is built upon thin film technology. Thin films are employed when only limited or very expensive bulk materials with the required properties are available. In this process, a thin film of the necessary material is evaporated, sputtered, plated, implanted, mixed, or sprayed onto a different carrier material. Neither the carrier material nor the deposited material needs to be electrically conductive [9].

"Despite the influence of residual gases in the recipient, and that of the coating material and the condensation rate, the entrapping residual gas molecules into the film can be kept arbitrarily small, if only the residual gas pressure in the recipient is kept accordingly low. Therefore, the conception of the vacuum system during the design and technical execution of vacuum coating plants for Physical Vapor Deposition (PVD) procedures is especially important" [9].

In figure 4.7, an old, once commercially available all-in-one vacuum evaporation setup is depicted.

Figure 4.7.: Edwards E306 vacuum evaporation setup. Source: Ernst Pölzler

5. Practical tests with a limited budget vacuum setup

5.1. The process of building an automated high vacuum setup

Constructing an automated high vacuum setup is undoubtedly a challenging endeavor, requiring a diverse set of skills. This skill set encompasses a profound understanding of high vacuum physics, proficiency in electrical engineering, and some familiarity with software development. Additionally, prior hands-on experience in vacuum physics (such as participation in a trainee program) would be advantageous. The timeline of the development of the vacuum setup can be found in appendix A.

One may discover that purchasing new vacuum appliances is prohibitively expensive. Fortunately, old industrial vacuum pumps as such are easily obtainable at second-hand markets. However, since these items are mostly in an undefined state, it poses a risk regarding the condition of the equipment one may acquire.

During the construction of the setup, several sensors were purchased, the majority of which were from Edwards. These sensors typically remain in good condition and offer excellent performance relative to their cost. The sensors are depicted in figure 3.1.

Selecting a roughing pump proved to be straightforward, as many options, even on the used market, were still prohibitively expensive upon research. One type stands out as particularly common and cost-effective: the rotary vane pump. The ideal companion for the size of the turbo pump used in the setup would certainly be a scroll vacuum pump, given that this type of pump operates without any oil.

The selection of the turbo pump was more opportunistic than deliberate, as much of the time was spent awaiting favorable offers on the second-hand market. Two different models were acquired in the process: the first being an Alcatel 5150, an older pump operating at a relatively low speed of 24,000 RPM, and the second being a Leybold Heraus Turbovac 360 with its original Turbotronik NT 150/360 driver.

A valve was employed to prevent accidental air backflow in the event of a power loss of the backing pump, as such an occurrence would lead to a catastrophic failure of the turbo pump.

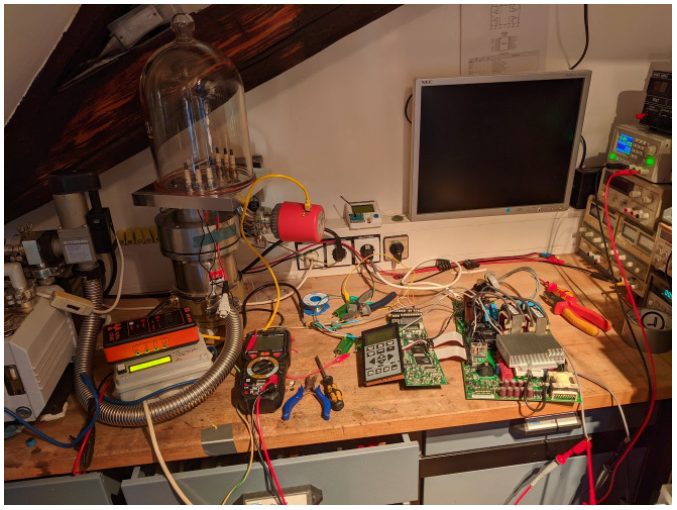

Figure 5.1.: The first high vacuum setup. Source: Sally Marcher

In figure 5.1, the first constructed vacuum setup is depicted. It consists of a rotary vane pump, two vacuum sensors from Edwards, and the older Alcatel 5150 pump, for which no documentation could be found aside from some product sheets. The driver, situated in the right part of the picture, consists of a modified frequency converter that could be sourced from an electronics dumpster. This converter was hacked to accept 60V input, which is suitable for this pump. Originally, the frequency converter only accepted 230V 3-phase input, but with a modification to the input voltage divider, it accepted the 60 volts. This required reverse engineering of the frequency converter, which was definitely one of the more challenging tasks.

The aluminum plate was manufactured at a CNC milling company in Innsbruck. To accomplish this, a plan was drawn, depicted in figure 5.2, using freeCAD, an open-source program designed for creating professional 3D models and plans. Subsequently, the aluminum plate, designed with spark plugs for electricity pass-throughs and mounting for the turbo pump and sensors in mind, was manufactured.

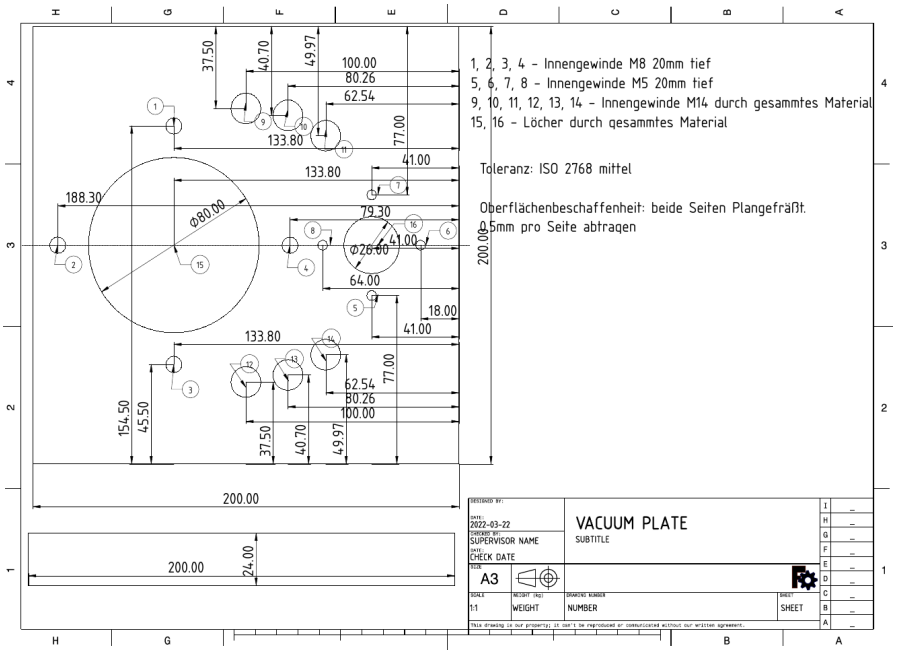

Figure 5.2.: The CNC milling plans. Source: Sally Marcher

The glass jar was acquired from Conatex, a supplier recommended to me by my physics teacher and supervisor of this paper, Professor Lackner.

Figure 5.3.: The final setup. Source: Sally Marcher

Soon, the setup required the entire table, and as this was not the only experiment in this laboratory, a solution regarding space usage had to be found. The solution was to build the setup into a different table, as depected in figure 5.3, along with an electronics installation box. With this final design, the Turbovac 360 unit was swapped out for the turbo pump, as it came with a driver, simplifying the setup.

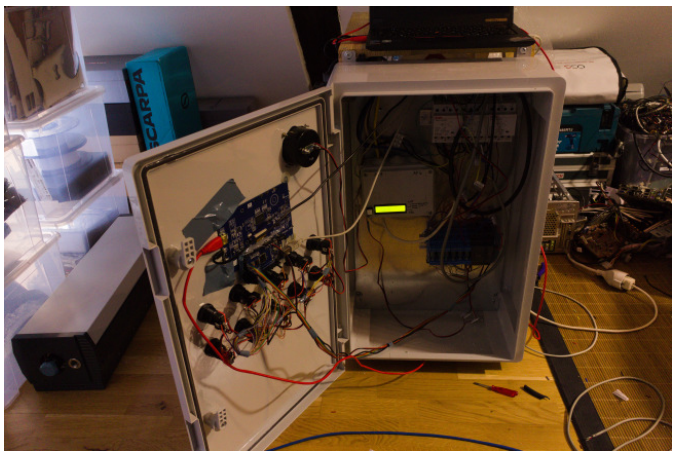

Figure 5.4.: The final setup electronics. Source: Sally Marcher

Since the setup needed to be automated, some electronics with a microcontroller had to be constructed. Because isolation was crucial when working with mains voltages, the use of opto-isolators, relays, and contactors was necessary. The sensor control box utilizes an ESP32 to read the voltage output of the sensors, as described in their datasheets.

The main control is managed by an Arduino Mega, as numerous inputs and outputs were required for the buttons, LEDs, and relays. Currently, the screen is connected to a laptop, but it will soon be integrated with a Raspberry Pi to read sensor values and document them.

The buttons on the front of the unit serve as the human interface device, providing control over every aspect of the setup.

The software development was carried out using the Arduino IDE for the ESP32 and Arduino Mega, and Python with curses for the application on the small touchscreen. All software is available on GitHub [28].

5.2. Pumping down to high vacuum

The purpose of this experiment is to investigate the behavior of pressure within a high vacuum environment over time. By systematically monitoring pressure changes, we aim to gain insights into the dynamics of pressure reduction and the factors affecting this process. Specifically, we will focus on observing the exponential decay of pressure as the

system evacuates, as predicted by the ideal gas law.

Understanding the behavior of pressure within high vacuum systems is not only of theoretical interest but also holds practical implications for the design and operation of vacuum equipment. By elucidating the dynamics of pressure reduction, this experiment aims to contribute to the understanding and research of vacuum technologies across various fields of application.

5.2.1. Materials and Methods

This experiment primarily utilizes the vacuum setup previously described, as depicted in figure 5.3. The setup comprises a rotary vane vacuum pump, a Leybold TURBOVAC 360C turbomolecular pump, an Edwards APG-M active Pirani gauge, an Edwards AIM active inverted magnetron gauge, and various vacuum adapters.

Both sensors are continuously read by specifically written software.

Only the rotary vane pump is operated until the vacuum chamber reaches a pressure slightly below the maximum foreline pressure of $5 \times 10^{-1} hPa$ to prevent any damage to the turbomolecular pump as it ramps up to its full operational speed of $45,000 rpm$ [31]. Once this pressure is reached, the turbomolecular pump can be started, initiating the pump down to high vacuum.

$$p \cdot V = n \cdot R \cdot T \tag{5.1}$$

where:

p ... Absolute pressure [Bar]
V ... Volume [L]
n ... Number of moles of gas [n]
T ... Temperature in Kelvin [K]
R ... Gas constant [J/mol K]

Utilizing equation (5.1) [16] and certain assumptions — specifically, having the same number of moles of gases in the system and constant temperature — the simplified version given by equation (5.2) may be employed. This is not an accurate representation, as with a decrease in pressure, the temperature must also decrease. However, this effect will be neglected, as it only makes a small difference at very low pressures [16].

$$p \cdot V = const \tag{5.2}$$

Now, we can conceptualize the vacuum setup as continually increasing in size with the specific pumping speed of the pumps. We will neglect factors such as gas dependence on pumping speed, as this would exceed the scope of this paper.

Furthermore, we will utilize the pumping speed of the roughing pump, which is $0.75 L/s$ [5], until a pressure of $1 \times 10^{-1} hPa$ is reached. Subsequently, we will utilize the pumping speed of $340 L/s$ for the turbomolecular pump (TPM) [31]. It should be noted that this approach introduces some inaccuracy, as the TPM is not switched on exactly at that moment.

The simulation is implemented using Python and the source is available in appendix B.

5.2.2. Results

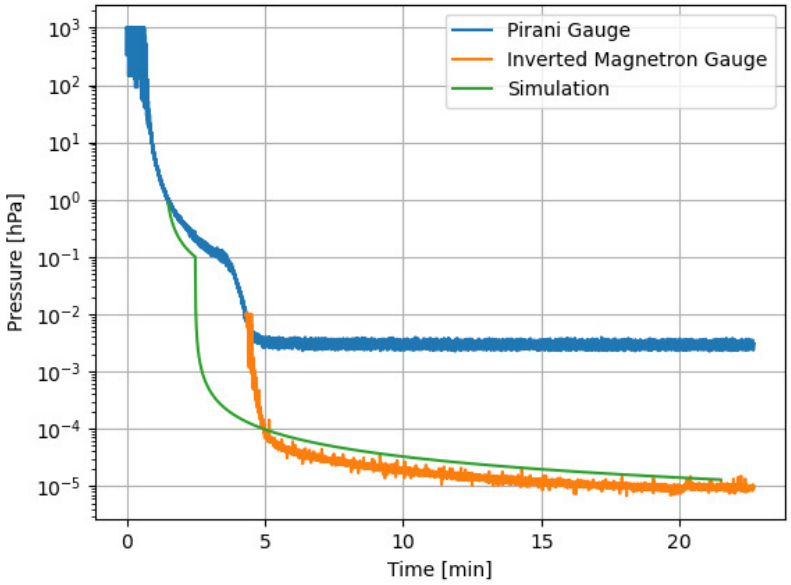

Figure 5.5.: Experiment results. Source: Sally Marcher

The lowest achieved pressure measured was 6.7×10^{-6} mBar, which is definitely within the lower end of high vacuum.

5.2.3. Discussion

The simulation cannot accurately describe this process, especially under higher pressures. Therefore, the simulation was limited to pressures below $1hPa$, for which it was surprisingly accurate up to a certain point. Namely, at extremely low pressure levels, as described at the beginning of this paper. The process of pumping to high and ultra-high vacuum is more akin to a statistical game of capturing gas molecules than a process that can be described with the ideal gas formula.

The significant gap in the intermediate pressure level, particularly at the threshold of the turbo pump, can be attributed to the substantial startup time of the high vacuum pump, which is 2 minutes. This phase was neglected during the simulation, as accurately describing it would require advanced statistical calculations and additional measurements, which would undoubtedly exceed the scope of this paper.

Regarding the practical issues with this setup, the seal between the aluminum and the glass jar is currently the biggest bottleneck. Vacuum grease, known for its poor vacuum performance, is currently used as a seal between aluminum and glass. This should be replaced with a plastic material like FKM, which is known for its excellent vacuum performance.

Seals play a significant role at such extreamly low pressures, and the choice of seal material can have a substantial impact on the performance of the entire setup. With this in mind, future improvements are definitely possible.

6. Conclusion

The construction of the vacuum setup has undoubtedly been a success, achieving a pressure of 6.7×10^{-6} mBar, firmly placing it within the high vacuum region. The construction process was lengthy, spanning over four years and incurring expenses within the four-digit range.

The theoretical part of the paper was intentionally simplified to provide the basics, as delving deeper into certain principles would exceed the scope of this paper. Much of the foundational knowledge was gleaned from literature, with valuable insights gained through the hands-on experience of constructing a vacuum setup.

6.1. Lessions learned

6.1.1. Bearrings

The bearings of turbo molecular pumps are meticulously constructed to withstand rotary speeds of up to 90,000 rpm [23]. Manufactured with precision using special ceramics and tight tolerances, these bearings eventually wear out over time, and servicing them can be prohibitively expensive. For instance, Leybold quoted €2200 without tax and shipping for servicing the TURBOVAC 360 [8]. Fortunately, there are resources available that provide guidance on safely replacing bearings in turbo molecular pumps [8], and the bearings themselves can be obtained from various websites, with attention paid to the required rotational speed.

Regarding lubrication for these bearings, oil diffusion pump oil can be used for oil-lubricated turbo pumps [8]. For grease-lubricated pumps like the TURBOVAC 360, "Ballistol Universalöl" was chosen due to its evaporative properties under vacuum, leaving behind an appropriate amount of grease for proper operation.

6.1.2. Electrical contactors and inrush current

Unfortunately, one vacuum valve was electrically damaged during the construction of the vacuum setup, necessitating repairs. The fault occurred due to the high inrush current of the engaging coil of the valve. This valve comprises two coils: one low-impedance, high-current coil responsible for engaging the valve, and a second high-impedance, low-current coil for holding the valve open, minimizing power loss to heat.

The electronics controlling the timing are not designed to handle rapid changes in the supplied voltage and would fail catastrophically in such cases. Initially, a relay board was employed to switch the 230V supply for each component of the vacuum setup, including this valve. While the relays were rated for 6A, it was discovered that the bouncing

effect of the relays, combined with the high inrush current, led to a catastrophic failure. Initially, the relay failed, followed quickly by the electronic components of the valve blowing up.

This issue could have been resolved by modulating the input signal to the relay [26]. However, opting for proper contactors rated for 40A provided a faster solution, albeit at a higher cost.

6.1.3. Do not trust strangers on the internet

"If a deal seems too good to be true, it probably is." [14]. This adage became particularly relevant during the construction of the vacuum setup, where social skills played a crucial role. Even for oddly specific listings, such as high vacuum devices, scams abound on the second-hand market. Identifying these fraudulent listings typically involves interacting with the seller; if they demonstrate a lack of knowledge about the device they are selling, it is wise to exercise extra caution.

6.1.4. Building networks

Extremely knowledgeable individuals played a crucial role in the development of my high vacuum setup. From learning how to draw ISO-specified plans to debugging vacuum pump controllers from Leybold, a multitude of people offered invaluable assistance, leading me to develop new problem-solving skills. Along the journey, many friendships were forged, although some were lost due to the time constraints of such a complex hobby. Overall, this experience has reshaped my way of thinking in everyday life, providing a more secure outlook on my career and fostering connections within new communities.

6.2. Special Thanks

- Bernd Lackner: Supervising teacher
- Jasmin Zweytick: VWA mentor at UNI Graz
- My parents: For giving me space for my experiments
- Daniel Plank: For organizing the CNC milling in Innsbruck and helping me with electrical standards
- Ilya Kirillov: For the titlepage artwork
- Peter Pötzi: For the electric contactors
- Ernst Pölzler: Providing photos and documentation of a vacuum evaporation setup
- Leybold GmbH: Providing me information about TURBOVAC 360C
- Pfeiffer Vacuum GmbH: Responding to my email about the QMG111B

A. Construction timeline

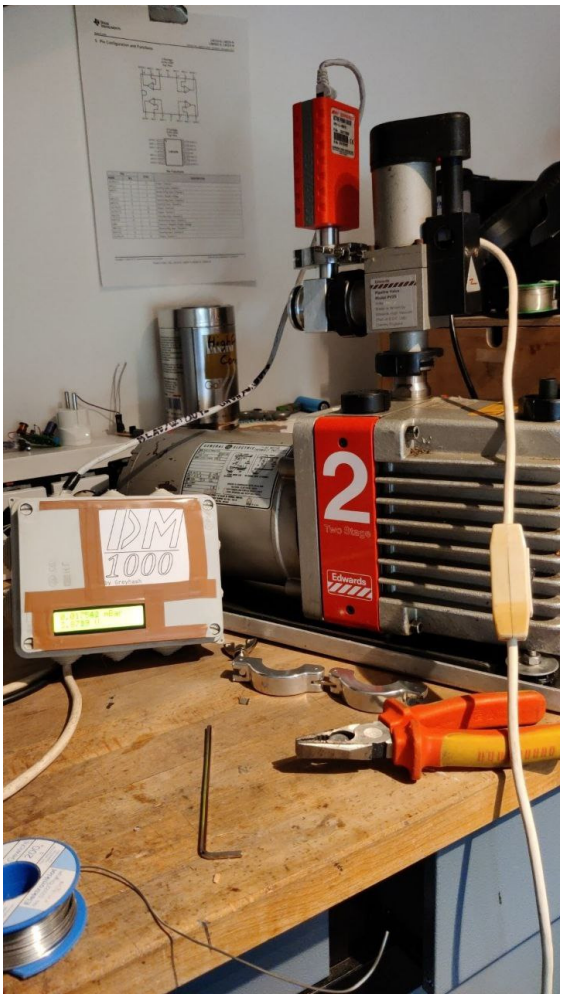

Figure A.1.: 18. Sep. 2021

The initial recorded tests with the Edwards E2M2 rotary vane pump commenced in September 2021. At that time, the only meter available was the Edwards APG, which facilitated the acquisition of fundamental insights into rotary vane pumps. The electronics for the meter were designed and built by me at that stage, and portions of the code remain in use to this day.
It is worth noting that the very first tests were conducted earlier in 2021; unfortunately, no pictures from that phase have remained.

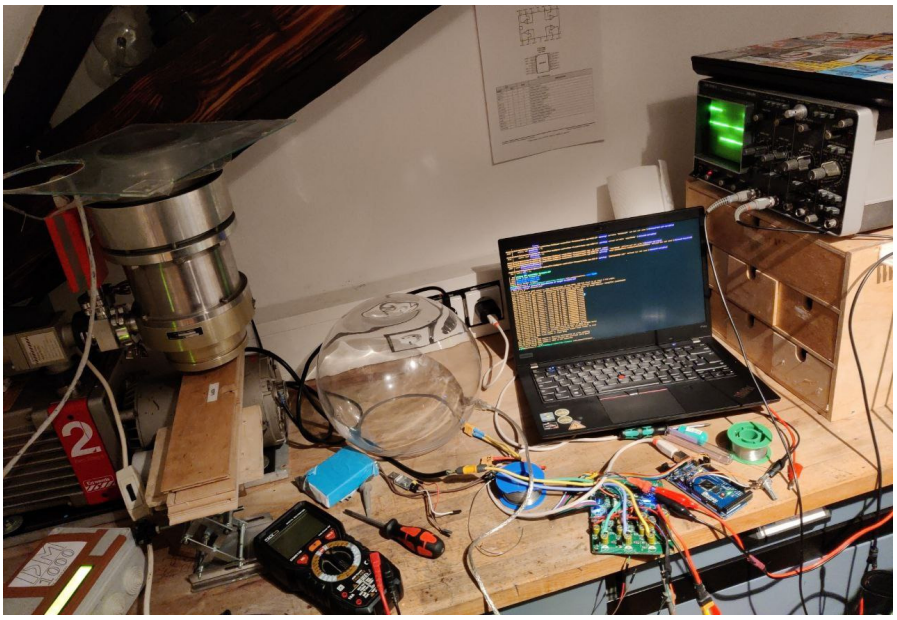

Figure A.2.: 4. Oct. 2021

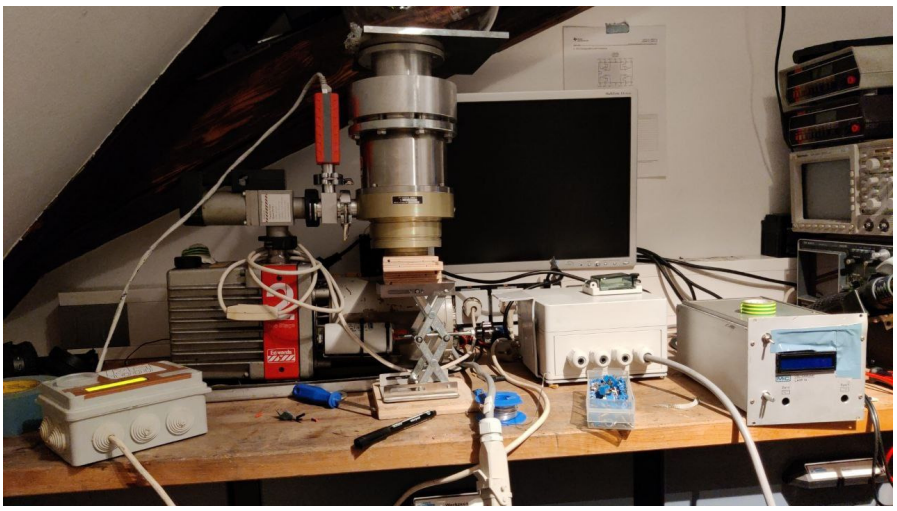

Figure A.3.: 1. Mar. 2022

With a new investment, a turbo molecular pump was soon acquired. The Alcatel 5150 posed a challenge to get running smoothly. Official documentation was unavailable, and only a limited amount of data could be found. Unfortunately, Alcatel did not respond to my emails regarding this pump. The driver depicted was the first version, self-designed and built for the purpose of powering electric bobby cars with up to 5 kW of power. The voltage range was approximately suitable, some minor modifications to both hardware and software were necessary to ensure the pump operated effectively.

After obtaining another Edwards sensor, the active inverted magnetron gauge, it became necessary to build a new vacuum chamber with a KF-25 flange mount. Additionally, electrical passthroughs in the form of spark plugs were incorporated into the design. The plans were created using FreeCAD, and the part was manufactured on a CNC machine in Innsbruck.

Figure A.4.: 17. Apr. 2022

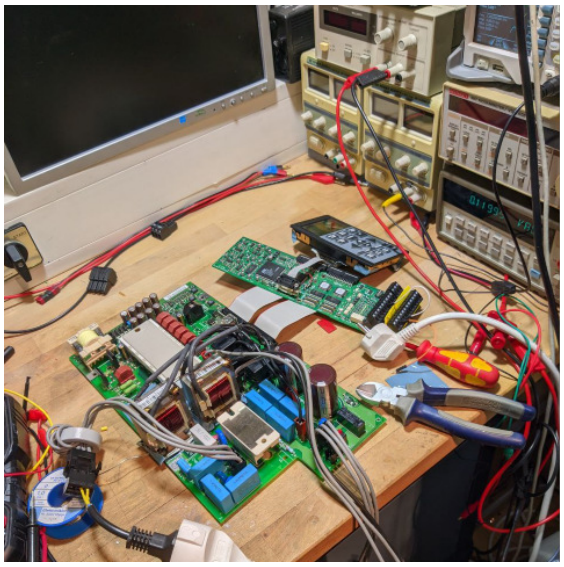

The first version of the DIY driver malfunctioned due to overvoltage resulting from resonance during pump deceleration. The replacement driver was constructed from a frequency converter salvaged from discarded equipment. Following extensive reverse engineering and minor modifications, it successfully powered the Alcatel Pump reliably.

Figure A.5.: 5. Oct. 2022

Figure A.6.: 9. Oct. 2022

With the addition of a new vacuum-rated glass jar, experiments could safely be conducted under vacuum conditions, replacing a previous container that posed safety risks. One of the initial experiments involved generating X-rays. The blue light emitted results from ionized gas formed by high-energy electrons colliding with residual gas. In this scenario, the turbo pump was not activated, as the roughing pump alone could attain sufficient vacuum levels.
It is important to highlight that safety measures were implemented for radiation safety and handling high voltage.

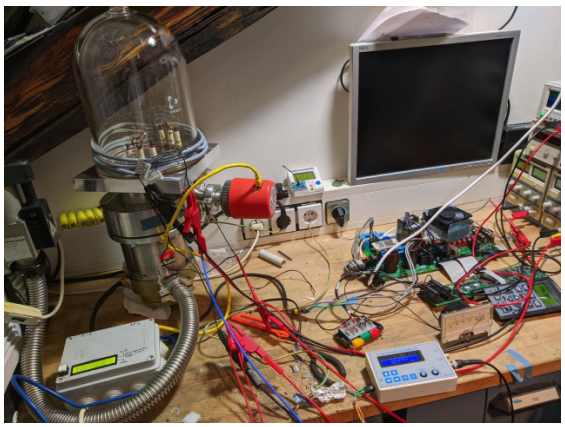

Figure A.7.: 7. Nov. 2022

Further experiments involved electron guns, serving as a source of free electrons that are emitted in a defined beam with a specific energy, dependent on the acceleration voltage. Magnetic fields were employed to manipulate the electron path.

Figure A.8.: 7. Mar. 2023

Figure A.9.: 7. Mar. 2023

With the arrival of the new TURBOVAC 360C, complete with a functioning driver, the old and clunky setup could be rebuilt in a cleaner and more user-friendly manner.

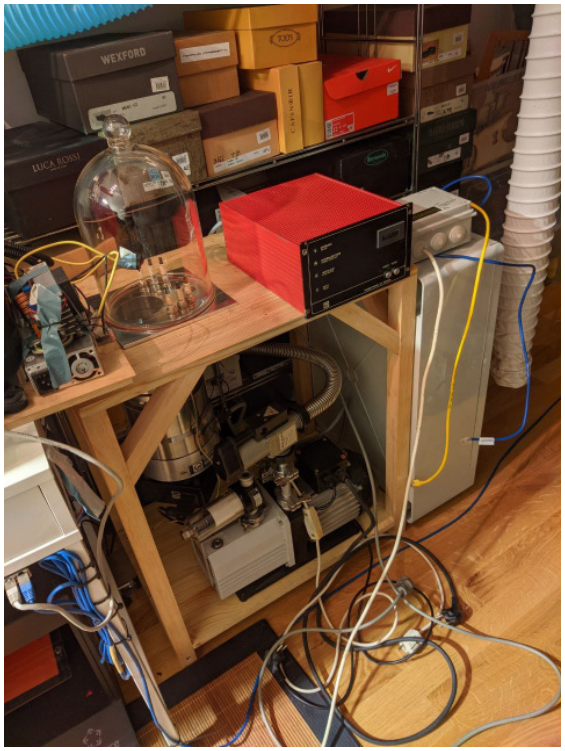

After operating on a tabletop for months, a final setup had to be constructed. Leveraging my woodworking skills, I built a sturdy table with the setup incorporated. However, the electronics still needed to be assembled.

Figure A.10.: 19. May. 2023

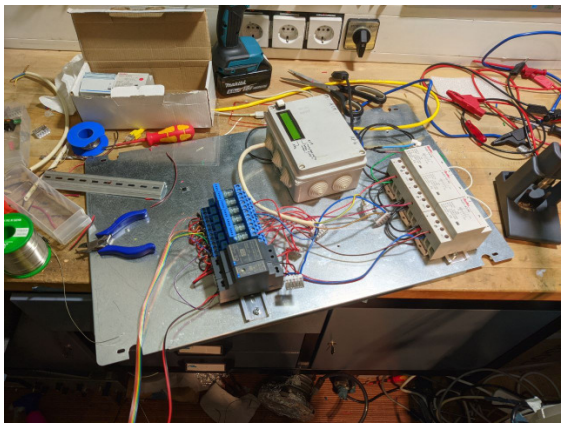

With this paper nearing its deadline, the final task was to fully automate the system. Until now, it has been operated manually, with components plugged in and cables connected with precise timing. This newly constructed box incorporates electrical contactors in two sizes, several power supplies, the sensor control box, and an Arduino Mega to control all operations.

Figure A.11.: 10. Feb. 2024

Figure A.12.: 10. Feb. 2024

The setup has been successfully completed, incorporating all necessary components and systems as detailed in the preceding sections.

The plan for electron beam lithography will be pursued in the future, although its inclusion in this paper is not viable due to the imposed deadline.

B. Simulation code

```
import matplotlib.pyplot as plt

vol = 10 # Initial Volume [L]
p = 1 # Initial Pressure [hPa]
inc_1 = 0.75 # Pumping speed by rotary pump [L/s]
thr = 1e-1 # Pressure threshold from inc_1 to inc_2
inc_2 = 340 # Pumping speed by tpm [L/s]

sim_len = 60*20 # Simulation duration [s]

const = p * vol

x = []
y = []

for i in range(0, sim_len):
  x.append(i/60)
  if(p > thr):
    vol += inc_1
  else:
    vol += inc_2
  p = const/vol
  y.append(p)

plt.plot(x,y, label="Simulation")
plt.yscale("log")
plt.yscale('log')
plt.ylabel("Pressure [hPa]")
plt.xlabel("Time [min]")
plt.grid('on')
plt.legend()
plt.show()
```

Listing B.1: Simulation code

List of Figures

Bibliography

[1] A. Ellett and R. M. Zabel. "The Pirani Gauge for the Measurement of Small Changes of Pressure". In: *Phys. Rev.* 37 (9 1931), pp. 1102–1111. DOI: 10.1103/PhysRev.37.1102. URL: https://link.aps.org/doi/10.1103/PhysRev.37.1102.

[2] J. P. Hobson and P. A. Redhead. "OPERATION OF AN INVERTED-MAGNETRON GAUGE IN THE PRESSURE RANGE 10-3 TO 10-12 MM. Hg". In: *Canadian Journal of Physics* 36.3 (1958), pp. 271–288. DOI: 10.1139/p58-031. URL: https://doi.org/10.1139/p58-031.

[3] W. V. Ligon. "Molecular Analysis by Mass Spectrometry". In: *Science* 205.4402 (1979), p. 151. DOI: 10.1126/science.205.4402.151. eprint: https://www.science.org/doi/pdf/10.1126/science.205.4402.151. URL: https://www.science.org/doi/abs/10.1126/science.205.4402.151.

[4] *Rotary Vacuum Pumps E2M2, E1/E2M5 and 8, E2M12*. A360-01-880. Rev. H. Edwards High Vacuum International. 1996. URL: https://www.idealvac.com/files/ManualsII/Edwards_E2M2_to_E2M12_Users_Instruction_Manual.pdf.

[5] *TRIVAC E 2*. GA 01.602/1.02. LEYBOLD VAKUUM GmbH. 2001. URL: https://www.idealvac.com/files/ManualsII/Leybold_D_E2_5OI.pdf.

[6] K Jousten. "Ultrahigh vacuum gauges". In: (2007). DOI: 10.5170/CERN-2007-003.145. URL: https://cds.cern.ch/record/1046855.

[7] *Metal Sealed Active Inverted Magnetron Gauge*. D146-61-880. Issue L. Edwards High Vacuum International. 2012.

[8] glasslinger Ron Soyland. *replacing bearings in a turbomolecular vacuum pump*. 2014. URL: https://www.youtube.com/watch?v=jL0fXUZ4wFQ (visited on 02/19/2024).

[9] H. Frey and H.R. Khan. *Handbook of Thin Film Technology*. Springer Berlin Heidelberg, 2015. ISBN: 9783642054303. URL: https://books.google.at/books?id=qrklCQAAQBAJ.

[10] P. Horowitz and W. Hill. *The Art of Electronics*. Cambridge University Press, 2015. ISBN: 9780521809269. URL: https://books.google.at/books?id=LAiWPwAACAAJ.

[11] K. Jousten. "Total Pressure Vacuum Gauges". In: *Handbook of Vacuum Technology*. John Wiley Sons, Ltd, 2016. Chap. 13, pp. 565–642. ISBN: 9783527688265. DOI: https://doi.org/10.1002/9783527688265.ch13. eprint: https://onlinelibrary.wiley.com/doi/pdf/10.1002/9783527688265.ch13. URL: https://onlinelibrary.wiley.com/doi/abs/10.1002/9783527688265.ch13.

[12] Leybold GmbH. *How does a turbomolecular pump work?* 2017. URL: https://www.leybold.com/en/knowledge/vacuum-fundamentals/vacuum-generation/how-does-a-turbomolecular-pump-work (visited on 10/12/2023).

[13] Jürgen H. Gross. "Instrumentation". In: *Mass Spectrometry: A Textbook*. Cham: Springer International Publishing, 2017, pp. 151–292. ISBN: 978-3-319-54398-7. DOI: 10.1007/978-3-319-54398-7_4. URL: https://doi.org/10.1007/978-3-319-54398-7_4.

[14] doktor pytaTopic. *Warning: !!! Metrology scam !!!* Forum. 2017. URL: https://www.eevblog.com/forum/metrology/warning-!!!-metrology-scam-!!!/ (visited on 02/19/2024).

[15] K. Akhtar et al. "Scanning Electron Microscopy: Principle and Applications in Nanomaterials Characterization". In: *Handbook of Materials Characterization*. Ed. by Surender Kumar Sharma. Cham: Springer International Publishing, 2018, pp. 113–145. ISBN: 978-3-319-92955-2. DOI: 10.1007/978-3-319-92955-2_4. URL: https://doi.org/10.1007/978-3-319-92955-2_4.

[16] D. Halliday, R. Resnick, and J. Walker. *Fundamentals of Physics, Extended*. Wiley, 2018. ISBN: 9781119460138.

[17] *CMR 371 ... CMR 375*. BG 5138 BEN / B. Pfeiffer Vacuum GmbH. 2019.

[18] N. Fu et al. "EUV Lithography: State-of-the-Art Review". In: *Journal of Microelectronic Manufacturing* 2 (June 2019), pp. 1–6. DOI: 10.33079/jomm.19020202.

[19] P. Lambretz. *Working with turbomolecular vacuum pumps*. 2019. URL: https://www.vacuumscienceworld.com/blog/working-with-turbomulecular-vacuum-pumps (visited on 01/03/2024).

[20] Vacuum Science World News. *Everything you need to know about scroll pumps*. 2019. URL: https://www.vacuumscienceworld.com/blog/everything-you-need-to-know-about-scroll-pumps (visited on 08/05/2023).

[21] Applied Science Ben Krasnow. *Giant glass diffusion pump and cathode ray tube demo*. 2020. URL: https://www.youtube.com/watch?v=SrNVLCHrJtY (visited on 08/24/2023).

[22] Vacuum Science World News. *Diaphragm Vacuum Pumps - how they work and where to use them*. 2020. URL: https://www.vacuumscienceworld.com/blog/diaphragm-vacuum-pumps (visited on 08/05/2023).

[23] *HiPace® 10 with TC 110, DN 25*. Pfeiffer Vacuum GmbH. 2023. URL: https://static.pfeiffer-vacuum.com/productPdfs/PMP03960.en.pdf.

[24] Reuters. *ASML ships first "High NA" lithography system to Intel -statement*. Dec. 21, 2023. URL: https://www.reuters.com/technology/asml-ships-first-high-na-lithography-system-intel-statement-2023-12-21/ (visited on 02/05/2024).

[25] *Trigon BCG552*. tinb77e1. INFICON Holding AG. 2023. URL: https://www.inficon.com/media/9695/download/Operating-Manual-Trigon%E2%84%A2-BCG552-TripleGauge%C2%AE.pdf?v=1&inline=true&language=en.

[26] Fabian Winkel et al. "Reducing Contact Bouncing of a Relay by Optimizing the Switch Signal During Run-Time". In: *IEEE Transactions on Automation Science and Engineering* (2023). DOI: 10.1109/TASE.2023.3322762.

[27] Pfeiffer Vacuum GmbH. *Turbopumps - the pacesetters among vacuum pumps*. 2024. URL: https://www.pfeiffer-vacuum.com/en/products/vacuum-generation/turbopumps/ (visited on 01/03/2024).

[28] Greyhash. *vacuum-stuff*. https://github.com/Greyhash-dev/vacuum-stuff. 2024.

[29] Zeiss. "High-NA-EUV: New technology for global microchip production". In: (Jan. 30, 2024). URL: https://www.zeiss.com/semiconductor-manufacturing-technology/news-and-events/smt-press-releases/2024/high-na-euv-lithography.html (visited on 02/05/2024).

[30] Leybold GmbH. *How does a rotary vane pump work?* URL: https://www.leybold.com/en/knowledge/vacuum-fundamentals/vacuum-generation/how-does-an-oil-sealed-rotary-displacement-pump-work (visited on 07/28/2023).

[31] UHV Tech Services Inc. *Leybold TURBOVAC 360 / TURBOVAC 360C*. Online Store. URL: https://uhvts.com/products/leybold-turbovac-360-turbovac-360c/ (visited on 02/13/2024).

Declaration of Independence

I, Sally Marcher, declare that this paper is entirely my own work. I affirm that I have authored this paper independently and have used only the sources and aids listed in the bibliography and acknowledgments.

I acknowledge proper citation for all external ideas, concepts, and data, adhering to academic standards. Any assistance received is duly acknowledged.

Sally Marcher	Date